Characterisation of precipitation microstructures in aluminium alloys 7040 and 7050 and their relationship to mechanical behaviour

D. Dumont, A. Deschamps, Y. Bréchet, C. Sigli and J. C. Ehrström

This paper investigates the precipitation microstructures in aluminium alloys 7040 and 7050 (Al–Zn–Mg–Cu variants) as a function of quench rate and aging treatment, and the associated compromise between yield strength and fracture toughness. The precipitate microstructures are quantitatively characterised by a combination of techniques covering the different scales involved: transmission electron microscopy (TEM), field-emission gun scanning electron microscopy (FEG-SEM) and small angle X-ray scattering (SAXS), and fracture toughness is estimated using the Kahn tear test. Yield strength and strain hardening behaviour are determined by conventional tensile tests. It is shown that the composition modification from alloy 7040 to alloy 7050 results in a better compromise between yield strength and toughness. The strength decrease in alloy 7040 following a slow quench is much reduced compared to alloy 7050 because of a lower sensitivity to quench-induced precipitation on dispersoids. Both alloys show a large decrease in toughness upon slow cooling, however this decrease is much more pronounced in the case of alloy 7050 because of the presence of bands of dispersoid nucleated quench-induced precipitates, promoting low energy transgranular fracture. Further improvement of toughness values in the slowly quenched materials would require a decrease in the quench sensitivity of grain boundary precipitation. MST/5778

Keywords: Aluminium alloys, 7040, 7050, Precipitation hardening, Toughness

Dr Dumont, Dr Sigli and Dr Ehrström are research engineers at the Pechiney Centre de Recherches de Voreppe, 725 rue Aristide Bergès, BP 27, 38 341 Voreppe Cedex, France. Dr Deschamps and Professor Bréchet are at the LTPCM/ENSEEG, CNRS–UMR 5614, Institut National Polytechnique de Grenoble, Domaine Universitaire, BP 75, 38 402 St Martin d'Hères Cedex, France (alexis.deschamps@ltpcm.inpg.fr). *Manuscript received 19 February 2003; accepted 14 January 2004.*

Introduction

Aluminium alloys of the age hardenable 7000 series are extensively used in aerospace applications where a good compromise between strength and damage tolerance is required.[1,2] The combination of these contradictory properties is governed by many mechanisms, each related to different characters of the microstructure.[3–5]

By concentrating on the sole precipitation microstructure, a number of precipitate types can have a determining role on the mechanical behaviour of the material:

(i) fine scale homogeneous precipitates govern the yield stress, through a complex relationship taking into account their size and nature;[6] they also have a large influence on the plastic properties of the material through the strain hardening rate,[7] and therefore on the energy dissipation during fracture[8–11]

(ii) intergranular precipitates, whether formed during the quench from the solution treatment, or during the aging treatment, control the strength and ductility of the grain boundaries, and therefore have a major influence on all intergranular fracture processes[12–16]

(iii) other quench-induced coarse precipitates (and notably those nucleated on dispersoids) have an indirect effect on yield strength by decreasing the available solid solution for further hardening precipitation,[17] and are potential sites for damage initiation in the grain interiors during a fracture process[18]

In the perspective of optimising a compromise of mechanical properties via microstructure control,[19] it is therefore necessary to understand quantitatively how all these microstructural features, which occur at vastly different time and length scales, are generated.

An optimisation of properties is reached by adjusting a number of parameters, such as composition, purity level control, and process parameters such as hot rolling schedules and heat treatment conditions. The development of new 7000 series aluminium alloys for thick plate applications is characteristic of this trend.[20] Traditional alloys of these series show a high quench sensitivity that is not compatible with the thick plates needed to produce modern aeroplane wings. Therefore, a new generation of alloys has been developed, with modified composition, which show a slightly smaller maximum strength but much higher service properties in a thick plate geometry.[21]

This paper is concerned with two alloys used for thick plate applications: 7050, which is a classical alloy used in aerospace applications, and 7040, which was recently developed to meet the need for increased plate thickness.[22,23] This paper aims to arrive at a detailed understanding of the difference in yield strength/toughness compromise in the light of a detailed study of the precipitate microstructures at all the necessary scales. This quantitative characterisation will be performed in a variety of process conditions, obtained by varying the quench rate as well as the aging treatment. In parallel with the microstructural study, the two main mechanical properties sought in the compromise, namely yield strength (and associated strain hardening) and fracture toughness (represented by the notch resistance) will be measured.

Experimental procedure

The composition of aluminium alloys 7040 and 7050 is given in Table 1. Alloy 7040 has a lower solute content (except in Zn), because it has been specifically designed for thick plate applications where a low quench sensitivity is required.

Both alloys were received as 150 mm thick plates from the Pechiney Centre de Recherches de Voreppe after rolling in the Pechiney Issoire mill. The material for the study was always taken between quarter thickness and 10 mm from the surface of the plate, in order to ensure a maximum homogeneity of composition and grain structure. The samples for microstructural studies and mechanical testing were 3 mm thick. They were first solutionised for 80 min, with a temperature ramp from 470 to 483°C. They were then quenched from 483°C with three different procedures: (a) cold water quench (fast quench rate labelled F, 850 K s^{-1}); (b) quench in boiling water (intermediate quench rate labelled I, 19 K s^{-1}); and (c) quench in boiling water, the sample being held between two 5 mm plates (slow quench rate labelled S, 7 K s^{-1}). The quench rates given here are initial values, which are valid down to approximately 250°C.

After quenching, the samples were held for 84 h at room temperature, ramped to 120°C at 30 K h^{-1}, left at 120°C for 6 h, ramped to 160°C at 30 K h^{-1}, and held for various times at 160°C. This two-stage heat treatment enables a good control of the hardening precipitate distribution, and is coherent with industrial practice. Three characteristic states were mainly studied: the Underaged (UA), peak aged (PA) and overaged (OA) conditions. The UA and OA conditions were chosen in all cases at a hardness value of 170 HV (yield strength approximately 470 MPa). The aging times at 120°C (for the UA condition) and 160°C necessary to achieve this hardness value, as well as the aging times for peak strength, are given in Table 2.

Samples for transmission electron microscopy (TEM) were prepared as follows: diamond saw cutting followed by mechanical grinding down to 120 μm, ultrasonic cutting of 3 mm disks, and electropolishing in a 1/3 nitric acid, 2/3 methanol solution held at −20°C, under a voltage of 15 V. Samples were observed with a Jeol 3010 microscope operating at 300 kV.

All SAXS experiments presented here have been carried out on the D2AM beamline of ESRF (BM02-CRG). X-rays are generated by a bending magnet, are focused and monochromated to better than $\delta\lambda/\lambda = 2 \times 10^{-4}$ at a wavelength of 1·492 Å. Acquisition was carried out with a 2D CCD camera. Two distances between the sample and camera were used, in order to maximise the measured q range. In this way, the scattering signal was measured in the range [0·001, 0·25] $Å^{-1}$, giving access to all types of precipitates present in the microstructure, from GP zones of about 1 nm diameter to coarse quench induces particles of about 200 nm diameter. Data files were corrected for electronic noise, flat field of the detector, and background noise. A circular average around the transmitted beam was carried out to obtain the intensity scattered at a given angle. The scattered intensity was finally converted into absolute values using a reference sample and the measurement of the intensity of the direct beam through calibrated filters. The precipitate size was evaluated by the Guinier approximation, and the precipitate volume fraction was evaluated assuming the equilibrium concentration for the precipitates $Mg(Zn,Cu)_2$. Details of the calculations for the radius and volume fraction can be found in Ref. 24.

Scanning electron microscope (SEM) observations were carried out at 10 kV on a SEM with a field emission gun (FEG) at Pechiney Centre de Recherches de Voreppe, on samples mechanically polished with a colloidal suspension of diamond at 0·25 μm.

The hardening potential was evaluated by microhardness indentation. Tensile tests were then carried out in the rolling direction on the main aging conditions at a strain rate of 5×10^{-3} s^{-1}, and the strain hardening capability of the material was measured by numerically differentiating the stress–strain curves. The notch resistance was evaluated using the Kahn tear test,[25–27] on 3 mm thick samples. The samples were loaded in the rolling direction, and the crack propagation was in the long transverse direction. Both the unit initiation energy (UIE) and the unit propagation energy (UPE) can be used to evaluate notch resistance. In all cases where fracture toughness is low (low quench rates), the UPE was found to be extremely small and not representative, whereas it was checked through selected tests on CT samples that the UIE was proportional to K_Q^2 in a wide range of process conditions. Therefore it is the UIE that will be used throughout this paper. Details of the experimental procedure for these notch resistance tests can be found in Ref. 28.

Table 1 Composition of alloys 7040 and 7050 in wt-%, balance Al

	Zn	Mg	Cu	Zr	Fe	Si
7040	6·51	2·01	1·64	0·11	0·08	0·05
7050	6·33	2·46	2·2	0·11	0·1	0·08

Characterisation of the precipitate microstructure at the different scales

In service conditions, the particles present in the microstructure of alloys 7040 and 7050 can be classified in four types, according to their different scales and spatial distribution: intermetallic constituent particles, formed during the early process, dispersoids, formed during homogenisation and hot rolling, coarse quench-induced precipitates, intergranular precipitates, either formed during the quench from the solution treatment or during the aging treatment, and fine hardening precipitates formed during the aging treatment. This section details their respective characteristics as functions of alloy nature, quench rate and aging condition.

INTERMETALLIC CONSTITUENT PARTICLES

The intermetallic particles present in both alloys consist mainly of Al_7Cu_2Fe, as well as undissolved Mg_2Si. The overall area fraction as measured from SEM observations is 0·6% for 7040 and 0·9% for 7050. It is expected that this lower content in intermetallic compounds for alloy 7040 will tend to increase its fracture toughness as compared to 7050.[29,30] However, these particles are not modified either by quench rate or aging treatment and therefore they will not be investigated further here.

Table 2 Summary of aging treatments used to generate the under, peak and overaged conditions for both alloys and three quench rates

Alloy	Quench rate	Underaged	Peak aged	Overaged
7040	Fast	1 h at 120°C	3 h at 160°C	21 h 30 min at 160°C
	Intermediate	1 h 30 min at 120°C	5 h at 160°C	21 h 30 min at 160°C
	Slow	1 h 30 min at 120°C	7 h at 160°C	23 h at 160°C
7050	Fast	1 h 40 min at 120°C	5 h at 160°C	60 h at 160°C
	Intermediate	1 h 40 min at 120°C	7 h at 160°C	40 h 30 min at 160°C
	Slow	1 h 30 min at 120°C	6 h at 160°C	41 h at 160°C

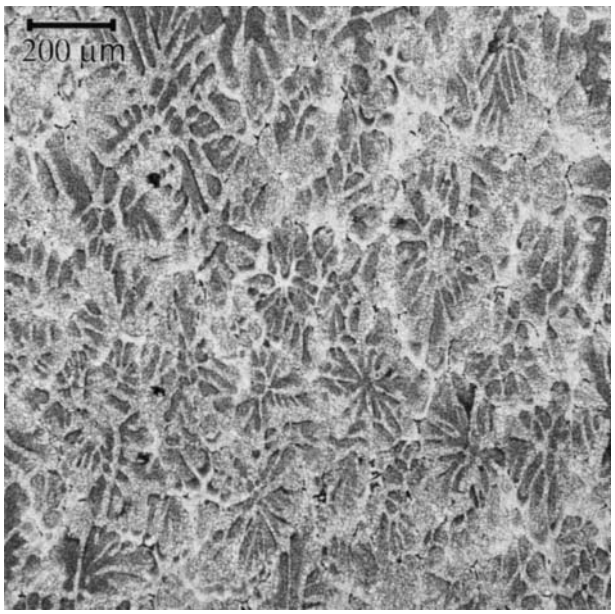

1 Microstructure of alloy 7050 after a slow quench: optical micrograph after orthophosphoric etching revealing the distribution of quench-induced particles. These particles are located in the high density regions of Al_3Zr particles, i.e. in the former dendrite interiors of the solidification microstructure, flattened by the rolling process

COARSE TRANSGRANULAR QUENCH-INDUCED PRECIPITATES

When the intermediate or slow quench rate are used, coarse η precipitates are observed inside the grains. These particles are nucleated on the Al_3Zr dispersoids.[17,31] These dispersoids are distributed heterogeneously in the material (mainly in the core of the solidification dendrites, because of the peritectic nature of Zr) as are the quench-induced precipitates. In Fig. 1, η particles are revealed by orthophosphoric acid etching. It is observed that the particles are distributed in bands, resulting from the solidification dendrite arms flattened by the rolling process.

TEM observations show the banded distribution of these precipitates in more detail. In alloy 7040, no bands are observed after a fast quench and after an intermediate quench only very occasional bands are observed, whereas after a slow quench well-defined precipitate bands are present (Fig. 2*a*). In contrast, for alloy 7050 a well-defined band structure is observed after an intermediate quench, and after a slow quench the material is extensively covered with coarse quench-induced precipitates (Fig. 2*b*). This is confirmed on a much larger scale by FEG-SEM observations, as shown in Fig. 3.

Therefore it can be concluded that transgranular precipitates, nucleated on the dispersoids are much more quench sensitive in alloy 7050. This agrees with the fact that it is richer in solute elements. However, it is not possible to rule out that the two alloys show different coherency of the dispersoids/matrix interface, notably because of differences

Table 3 Largest dimension (in nm) of transgranular quench-induced precipitates, determined from TEM and FEG-SEM images: standard deviation of the measurements is of the order of ± 30 nm

		Underaged		Overaged	
Alloy	Quench	TEM	FEG-SEM	TEM	FEG-SEM
7040	Slow	190	200	180	250
7050	Intermediate	205	180	200	210
	Slow	260	270	210	230

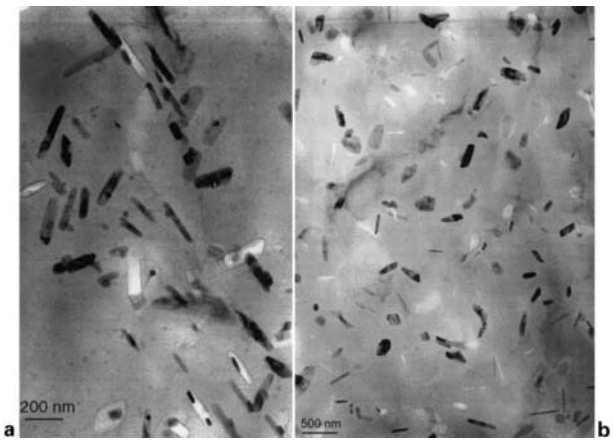

2 Bright field TEM micrographs of the microstructure of alloys *a* 7040 and *b* 7050 after a slow quench. Alloy 7040, which has a low quench sensitivity, shows narrow bands of coarse precipitates. Alloy 7050 is largely covered by wide bands of particles. The particle size is similar in both materials

in homogenisation practises, which could play a role in the quench sensitivity via the nucleation site efficiency.

A quantitative study of the precipitate size has been carried out with TEM and FEG-SEM. Table 3 shows the evaluation of the largest length of the particles as a function of alloy, quench rate and aging treatment. Both experimental techniques give very similar results in all cases. It is remarkable that no significant difference in particle size is detected in all the cases investigated (regardless of alloy or quench rate). TEM observations do not yield any difference and SEM observations only give a very small size increase from the intermediate quench to the slow quench. Therefore it appears that in the case of quench-induced particles the main difference between the two alloys and the two slower quenches (I and S) lies in the capability of Al_3Zr particles to act as nucleating sites. Once a particle is nucleated, regardless of alloy or quench rate, it grows to a size of about 200 nm.

A quantitative characterisation of the size and volume fraction of these coarse quench-induced particles has also been carried out by small angle X-ray scattering (SAXS) for the materials subjected to the fast and intermediate quench rates. Figure 4*a* and *b* shows the scattering curves for the two alloys and two quenches, in the overaged state.

Both alloys quenched at the fast rate do not show any sign of coarse particles: the only precipitates present with a significant volume fraction are the hardening precipitates, of radius 5–10 nm. For alloy 7050 quenched at the intermediate rate, it is observed that even though in this overaged state the hardening precipitates have coarsened to large sizes, they can be easily distinguished from the quench-induced particles which size is measured at 160 nm in diameter (Guinier approximation). This size, measured on a very large number of particles, is in very close agreement with the TEM and FEG-SEM observations above.

A striking difference between the two alloys is observed after the intermediate quench rate: alloy 7040 does not show any measurable fraction of coarse particles, whereas in the case of alloy 7050 the volume fraction of coarse particles can be estimated to 0·4%. For comparison, the surface fraction of coarse precipitates was evaluated in this condition by FEG-SEM to 0·44%. Again these two quantitative analysis, carried out on a comparatively large amount of material, are in complete agreement.

INTERGRANULAR PRECIPITATES

When the material is quenched in cold water, no intergranular precipitates are found. These develop during the

MST *(gamma)* MST38227.3d 9/3/04 18:10:57 Rev 7.51n/W (Jan 20 2003)

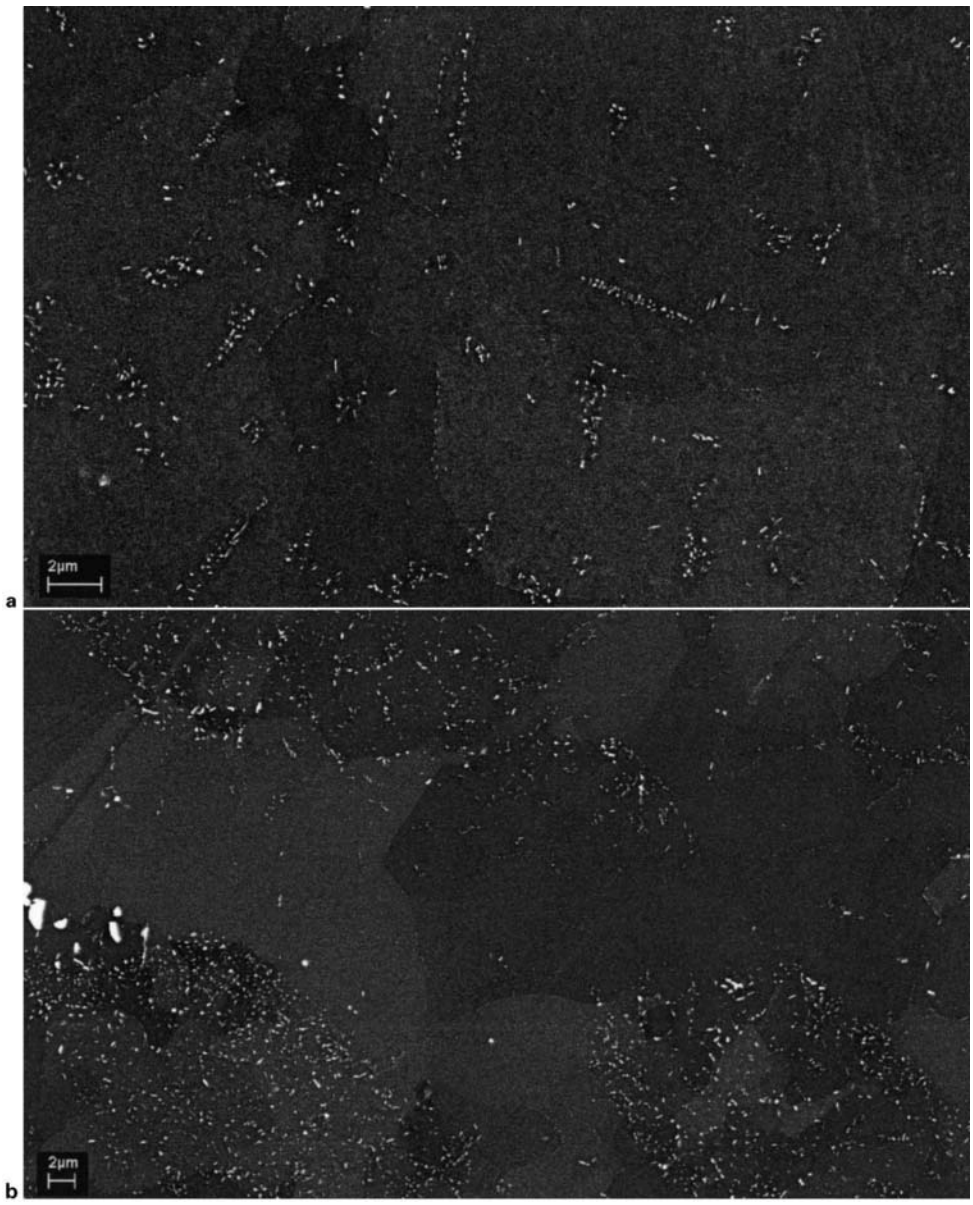

3 Backscattered electrons images in the FEG-SEM microscope of the microstructure of alloys *a* 7040 and *b* 7050 after a slow quench. These images confirm the large difference in the extent of the coarse particles bands between the two alloys. These bands have a limited extent in the case of alloy 7040, whereas they cover a large area in the case of alloy 7050

heat treatment at 160°C, as shown in Fig. 5*a* and *b* for both alloys. The average size of these intergranular precipitates was measured in the overaged state to be 40 nm, independently on the alloy (*see* Table 4).

After an intermediate quench, grain boundaries are densely covered with particles, as shown in Fig. 5*c* for alloy 7050. This is of course also the case for the slow quench. A quantitative analysis of the average size of these intergranular precipitates was carried out as a function of quench rate, alloy and state of aging (Table 4). It is observed that the precipitate size is independent of the state of aging because the aging temperature is too low to allow further particle growth. The particle size is also roughly independent of the alloy (except for the slow quench, where alloy 7040 shows a larger particle size), and increases when the quench rate is low. Although the two first conclusions match the behaviour of the coarse particles nucleated on the dispersoids, this last point is markedly different.

Table 4 Average largest precipitate dimension (in nm) on grain boundaries, measured on TEM micrographs: standard deviation of the measurements is of the order of $\pm$15 nm

Alloy	Quench	Underaged	Overaged
7040	Fast	...	40
	Intermediate	50	50
	Slow	80	110
7050	Fast	...	40
	Intermediate	60	50
	Slow	70	80

FINE HARDENING PRECIPITATES

During the two-step aging treatment, fine particles form homogeneously in the material. As usual in these alloys, the particles follow the sequence GP zones – η', metastable precipitates; η, precipitates.[32] GP zones are formed in the material during aging at room temperature and up to 120°C. During the 120°C heat treatment, η' precipitates form heterogeneously on the dissolving GP zones. At

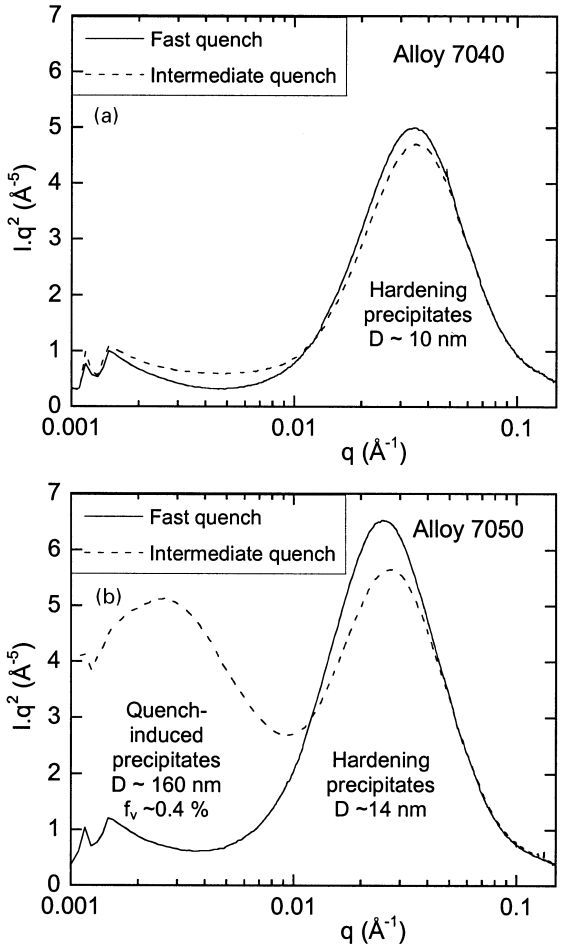

4 SAXS profiles (Iq^2 versus q) for both alloys, in the case of a fast and intermediate quench rate, and aged to the overaged state. In this graph, a maximum corresponds to a precipitate family, and the scattering vector q corresponding to this maximum in Iq^2 is inversely proportional to the average size of this precipitate family. The area under the curve $\int Iq^2 dq$ is proportional to the precipitate volume fraction of this given family. This figure shows that in the case of a fast quench none of the materials show a significant volume fraction of coarse particles. In the case of an intermediate quench, alloy 7040 still does not show any significant proportion of coarse particles, whereas alloy 7050 does

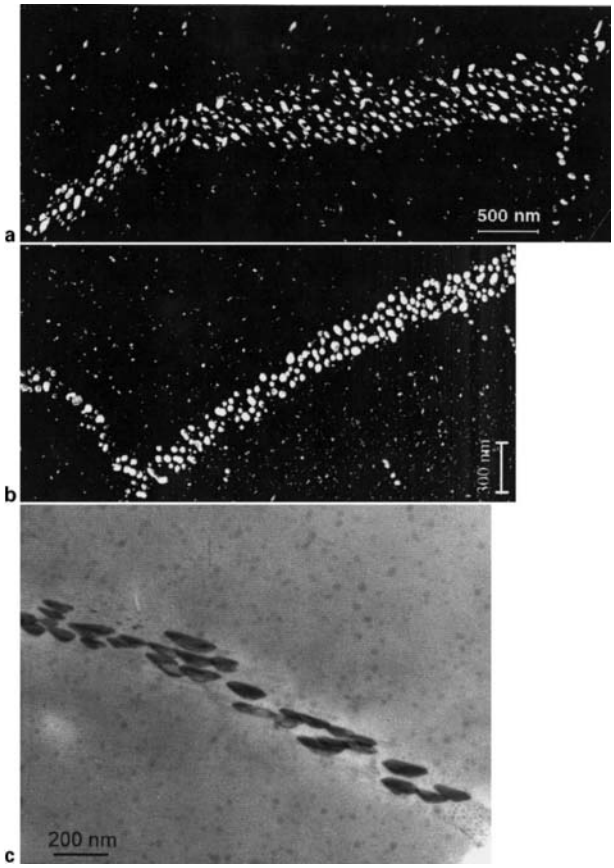

5 *a, b* dark field TEM micrographs of grain boundary precipitates in *a* alloy 7040 and *b* alloy 7050, after a fast quench rate and in the overaged condition; *c* bright field TEM micrograph of grain boundary precipitates in alloy 7040 after an intermediate quench rate and in the overaged condition

160°C, η' precipitates grow and are gradually replaced by the equilibrium phase η.[33]

A quantitative study of the size and volume fraction of these particles as a function of the alloy nature, quench rate and aging treatment has been carried out by SAXS. The results are presented in Fig. 6 for the precipitate radius and volume fraction, as a function of aging time at 160°C. It has to be pointed out that because of the way the different aging conditions were selected (i.e. peak aging at maximum hardness and under and over aging at a hardness of 170 HV), the aging times for each alloy and quench rate are necessarily different.

The precipitate size is almost independent of the quench rate in both alloys. This is quite surprising because after a slow quench the average solute content is much lower than after a fast quench, which should strongly affect the precipitation kinetics. However, as was shown by Deschamps and Bréchet in an earlier study,[17] the precipitation of coarse quench-induced precipitates depletes the solid solution in their immediate surroundings, creating a precipitate free zone (PFZ) around them, but leaves the rest of the material unaffected. Therefore, in the material far from quench-induced particles, the precipitation process occurs in a manner comparable to the rapidly quenched material.

It is apparent that the size of the precipitates are slightly larger in 7040, possibly owing to the higher Zn content (fast diffusing) and lower Mg and Cu contents (comparatively slower diffusing).

The evolution of precipitate volume fraction with aging time is shown in Fig. 6*b*. At peak strength both alloys show a comparable volume fraction, with minor differences. In both cases a slow quench rate results in a lower volume fraction of hardening precipitates. In the overaged condition, it is difficult to compare directly the two alloys because the aging times are very different. However, both alloys show a large decrease of the volume fraction associated with hardening precipitates when the quench rate is lowered. Lowering the quench rate reverses the order between the two alloys: after a fast quench, in the overaged condition, alloy 7050 shows a slightly higher volume fraction than alloy 7040, but this is no longer true after a slow quench. This illustrates the higher quench sensitivity of alloy 7050.

Characterisation of the mechanical properties

AGING CURVES

The hardening capability of the two alloys as a function of quench rate has been evaluated by hardness curves and the results are shown in Fig. 7. The overall effect of lowering the quench rate (and therefore forming coarse

MST *(gamma)* MST38227.3d 9/3/04 18:11:09 Rev 7.51n/W (Jan 20 2003)

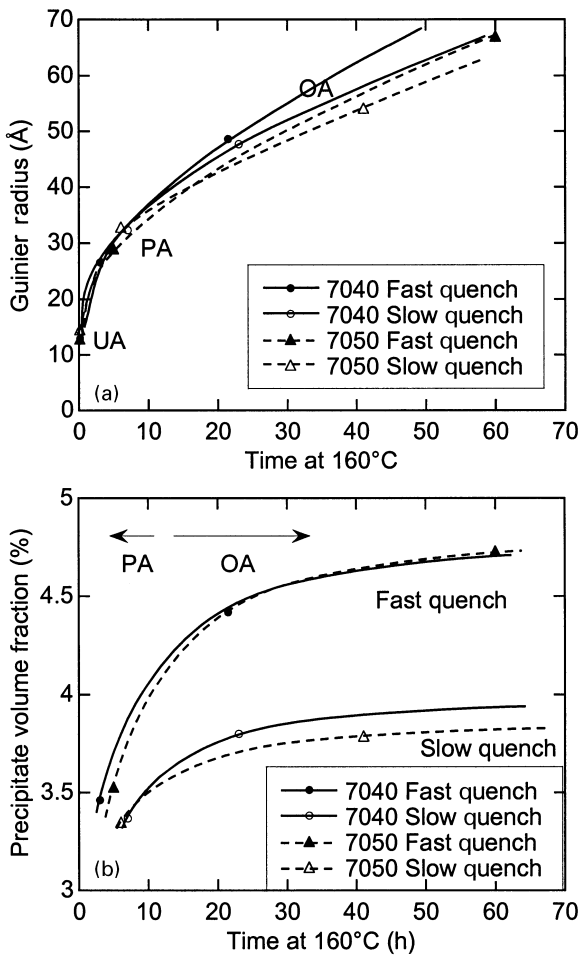

6 Quantitative determination of the hardening precipitates characteristics (namely size and volume fraction) in both alloys after a fast and slow quench, along the aging treatment (in the underaged, peak aged and overaged conditions)

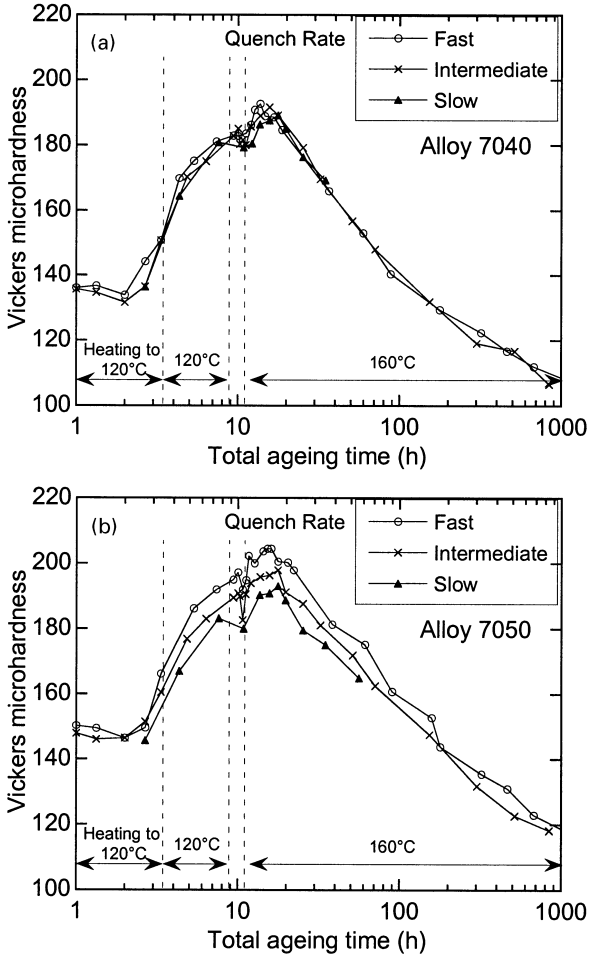

7 Aging curves determined by Vickers microhardness for both alloys and the fast, intermediate and slow quench rates. The lower quench sensitivity of alloy 7040 is clearly observed

non-hardening precipitates) is small, with a maximum decrease of hardness of about 10%. In alloy 7040 it is striking that there is almost no difference between the fast and slow quench. This is in agreement with the low quench sensitivity of this alloy. Logically, the 7050 alloy, which is more quench sensitive, shows a more pronounced decrease of hardness. Interestingly, this hardness decrease is constant over the complete aging curve, which is in agreement with the fact that the further precipitation kinetics are not much affected by the coarse induced precipitates.

STRAIN HARDENING

One parameter, which is expected to play a key role in notch resistance, is the strain hardening capability of the material. This strain hardening capability has been evaluated using tensile tests for both alloys, as a function of quench rate and aging condition. Results are shown in Fig. 8, in the form of Kocks–Mecking plots.[34,35]

The overall effect of aging on strain hardening is in agreement with previous work on similar systems.[7] In the Underaged condition the strain hardening rate is at its maximum, and at the end of the elastic–plastic transition it is still much higher than the classical stage II strain hardening rate ($\theta_{II} = \mu/20 \sim 1300$ MPa), probably owing to dynamic precipitation.[36] At peak aging the strain hardening rate is minimum, because of the depletion of the solid solution and the presence of shearable precipitates. In the overaged condition, the initial strain hardening rate increases again because of the accumulation of dislocations on non-shearable precipitates, however this is not maintained at large strains because of the depletion of the solid solution.

Both the alloy nature and the quench rate have only a minor effect on this strain hardening behaviour. For a given aging condition (i.e. UA, PA or OA), all curves superimpose almost exactly, except for alloy 7050, slowest quench rate, for which it is known that the volume fraction of coarse quench-induced precipitates is particularly high.

NOTCH RESISTANCE

Finally, the notch resistance has been evaluated for both alloys as a function of quench rate, all along the aging curve. This notch resistance (represented by the unit initiation energy UIE of the Kahn tear test) is plotted as a function of the yield strength, in order to provide some insight on the compromise between these two important mechanical characteristics. The results are shown in Fig. 9.

First of all, it is observed that after a fast quench, alloy 7040 shows a much higher notch resistance than alloy 7050. This effect may be attributed to a combination of two microstructural facts:

(i) higher content in constituent particles in alloy 7050
(ii) higher yield strength in alloy 7050.

After a slow quench, both alloys show a significant decrease of notch resistance. This detailed microstructural study suggests that this decrease is mainly due to two factors:

MST *(gamma)* MST38227.3d 9/3/04 18:11:13 Rev 7.51n/W (Jan 20 2003)

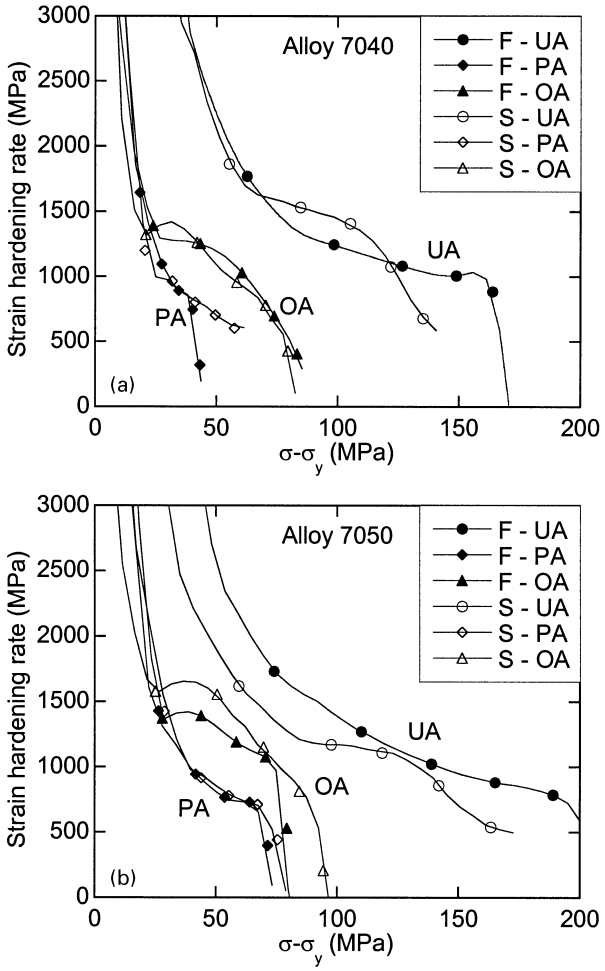

8 Strain hardening rate *v.* reduced stress curves for both alloys, fast (F) and slow (S) quenches, and the three aging conditions (under, peak, and overaged). The effect of alloy nature and quench rate appears to be of secondary importance as compared to the effect of aging treatment

(i) the decrease in the cohesion of grain boundaries caused by presence of coarse precipitates (identical for both alloys)

(ii) the decrease of the intrinsic toughness of the grain interiors caused by the presence of coarse quench-induced particles (largest for alloy 7050).

This is confirmed by the examination of the fracture surfaces of both materials in the Underaged condition following a slow quench (Fig. 10). Alloy 7040 shows mainly a mixture between shear transgranular fracture and intergranular fracture, which is characteristic of basically unperturbed grain interiors (leaving the possibility for macroscopic shear bands) associated with embrittled grain boundaries. Alloy 7050 shows a combination of the same intergranular fracture, but also ductile transgranular fracture nucleated on the many coarse quench-induced intragranular particles.

Other factors that could have influenced notch resistance are the yield strength and the strain hardening rate. Concerning the yield strength, it decreases when the quench rate is lowered, which should increase the notch resistance, while the strain hardening rate is almost unaffected by the quench rate.

As a consequence, after a slow quench rate, alloy 7040 shows a much better compromise between yield strength and notch resistance. Its notch resistance is lowered but still acceptable, and the yield strength is almost unchanged. On the contrary, alloy 7050 shows a very small notch resistance and a significant loss in yield strength.

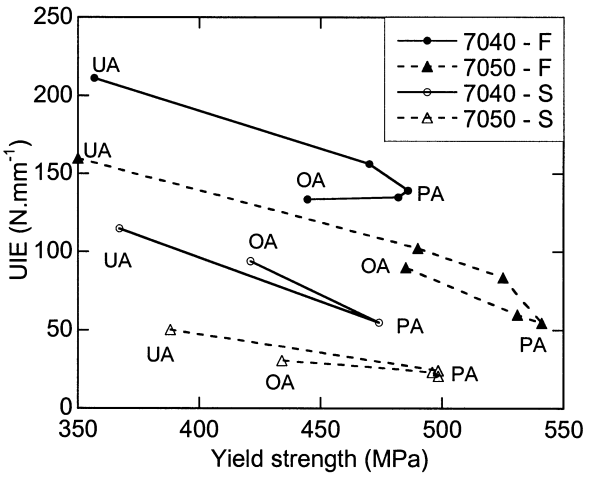

9 Unit initiation energy (UIE) measured from the Kahn tear tests, represented as a function of yield stress for both alloys, fast (F) and slow (S) quench rates, along the aging treatment

Finally, it is of interest to discuss the effect of aging on the notch resistance. In the case of a fast quench, the notch resistance is very high in the Underaged condition, lowest in the peak aged condition and increases again in the overaged condition. This is classically explained by the evolution of yield strength, precipitation on grain boundaries, the occurrence of a soft PFZ and the decrease in strain hardening, all occurring along the aging treatment.[37–39] The reduction in notch resistance from the under-aged condition to the peak aged condition can be attributed to the combination of a strain hardening rate decrease, an increased yield strength contrast between the PFZ and the grain interiors, and the development of grain boundary precipitates. The small increase in notch resistance between the peak aged and overaged conditions can be attributed to the reduced yield strength, associated with a small increase in strain hardening rate.

When the quench rate is lowered, the influence of the state of aging on the notch resistance is much less obvious. In the light of our microstructural study, this can be explained by the fact that with a slow quench grain boundaries are covered with coarse precipitates even in the as-quenched condition, and this parameter does not change significantly during the aging process. Therefore the residual influence of aging on notch resistance is only due to PFZ and strain hardening effects.

Discussion

We have concentrated our efforts on the characterisation of the different precipitate families, and have not considered other important microstructural features in relation with notch resistance such as the constituent particles or the grain structure. This choice is related to the process parameters studied here (quench rate and aging), which do not affect significantly the latter microstructural features, and which are of major importance in the development of a thick plate for aerospace applications.

The quench sensitivity of precipitation hardening aluminium alloys has been well studied in the literature, either for the purpose of predicting the strength[40] or for understanding the toughness and corrosion resistance in the quench and aged condition (quench factor analysis[41]):

(i) the quench factor analysis method developed by Staley and co-workers[18,41] uses a Johnson–Mehl–Avrami type of modelling for the precipitation

MST *(gamma)* MST38227.3d 9/3/04 18:11:14 Rev 7.51n/W (Jan 20 2003)

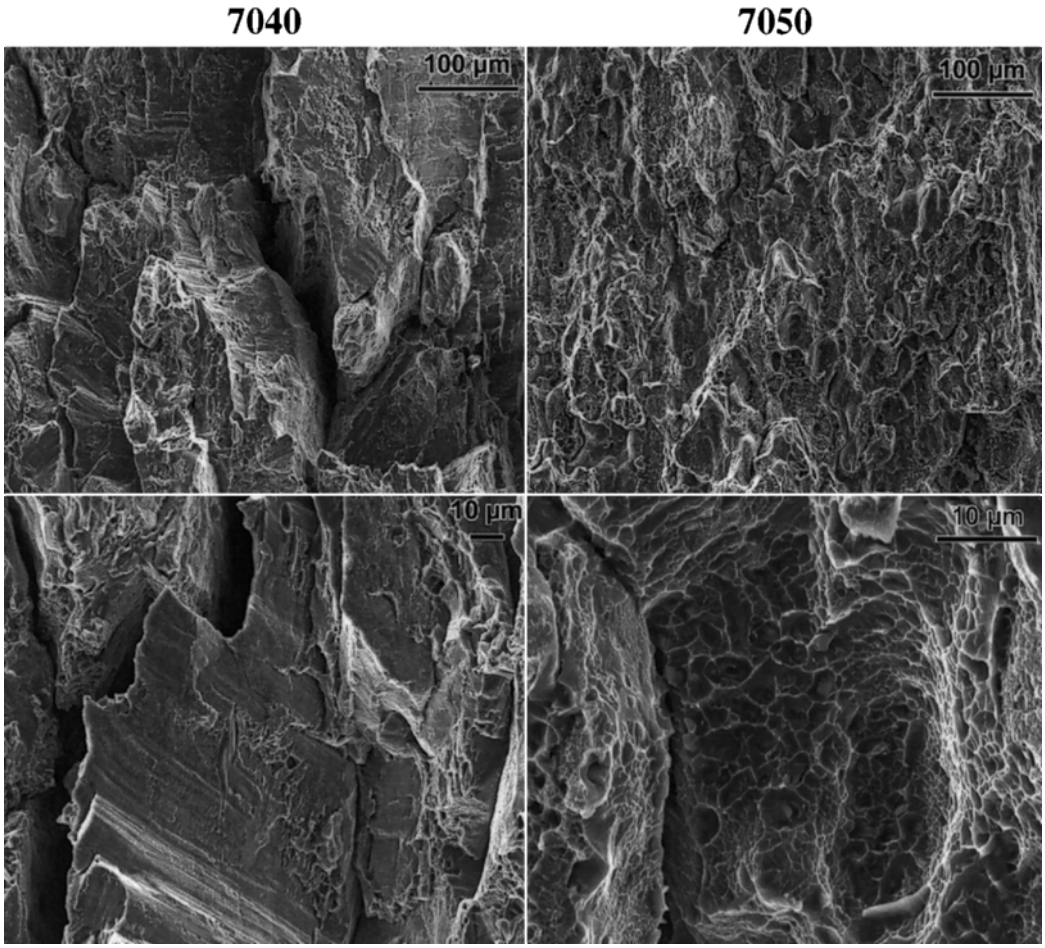

10 SEM micrographs of the Kahn tear test fracture surfaces for alloys 7040 and 7050 in the Underaged condition following a slow quench. Alloy 7040 shows mainly a combination of intragranular shear ductile fracture and intergranular fracture. Alloy 7050 shows mainly a combination of ductile transgranular fracture nucleated on the coarse quench-induced intragranular precipitates and intergranular fracture. The higher fraction of intermetallics on the fracture surface for this alloy is also apparent

kinetics during quenching, and the yield stress increase during post-quench aging is simply taken as proportional to the remaining solute. The loss in toughness observed when the quench rate is lowered is directly scaled with the loss in strength

(ii) the modelling approach developed by Bratland and co-workers,[40] which has been specifically used for predicting the post-quench hardening potential of 6000 series alloys, considers heterogeneous precipitation to nucleate on dispersoids during the quench, as was observed in the present case. However, the effect of quench-induced precipitates on the subsequent aging precipitation is modelled by considering a homogeneous material in which the solute content is the solute left over at the end of the quench.

In the light of these modelling approaches, the main experimental facts evidenced in the present study can be summarised, and some directions for further improvement of the models proposed:

(i) grain boundary precipitation and dispersoid nucleated precipitation are two separate problems, which need specific modelling treatments. In both alloys grain boundary precipitates observed after a given quench rate were quite similar in density, whereas the dispersoid nucleated precipitates were very sensitive to alloy composition. Moreover, the size of grain boundary precipitates depended on the quench rate, whereas the size of the dispersoid nucleated precipitates was similar, regardless of the quench rate. Specifically for the two alloys studied here, alloy 7040 meets the requirement of a low sensitivity to precipitation on dispersoids, but still shows significant precipitation on grain boundaries during a slow quench. This fact is responsible for a large part of its loss in notch resistance as compared to the fast quenched state, even though the loss in yield strength is negligible

(ii) the effect of dispersoid nucleated particles on post-quench aging and strengthening cannot be considered simply as a homogeneous depletion of the solid solution. It is shown that the precipitation kinetics (in terms of precipitate size) are not affected by a large volume fraction of quench-induced precipitates (alloy 7050, fast and slow quenches). Therefore, a correct assessment of the quench and aged state needs to consider the PFZs around the quench-induced particles, surrounded by mostly unchanged material

(iii) the effect of quench and aging on the evolution of notch resistance cannot be solely attributed to the strength loss. The complexity of the microstructure – notch resistance relationship is illustrated by the two following facts: (a) alloy 7050 shows a reduction of a factor of two in notch resistance between the fast and slow quenches, although the strength loss is only 10%; (b) alloy 7040 shows also a high loss in notch resistance in the same

MST *(gamma)* MST38227.3d 9/3/04 18:11:15 Rev 7.51n/W (Jan 20 2003)

condition, although no strength loss at all is observed. (In both cases, no significant change in work hardening rate with quench rate can be detected.) Therefore, both the grain boundary strength and the weakening of the grain interiors by bands of coarse precipitates appear to play a key role in controlling the toughness.

In an ideally quenched material, the evolution of notch resistance during aging is related to the combination of yield stress (high yield stress difference between the grain interiors and the PFZ promotes low notch resistance), strain hardening rate (the lower strain hardening rate in peak and overaged materials explains in part their lower notch resistance as compared to the Underaged material), and grain boundary precipitation during aging (which also accounts for the loss in notch resistance during the aging treatment).

When a modification of the microstructure is induced by a slow quench, the respective effects of these microstructural features on the notch resistance – strength compromise can be classified as follows:

(i) grain boundary precipitation occurring during quenching certainly has a very detrimental effect on notch resistance. This explains the loss in notch resistance when the quench rate is lowered for alloy 7040, which does not show significant dispersoid nucleated precipitation. It also explains the very low dependence of notch resistance with aging in the slowly quenched material. Grain boundary precipitation does not affect significantly the yield strength of the material

(ii) dispersoid nucleated precipitates also appear to have a strong influence on notch resistance. They favour nucleation and growth of voids inside the grains, and therefore decrease the intrinsic toughness of the grain interiors. These precipitates also play a prominent role in the strength loss, even though this strength loss is small compared to the loss in notch resistance. The improvement in the notch resistance – strength combination for thick plate applications when considering alloy 7040 instead of alloy 7050 is mostly related to a decrease in the alloy sensitivity to this type of precipitation. This decrease in sensitivity is in large part due to the compositional differences between the two alloys. However, another factor that cannot be ruled out is a change in the size and/or coherency of the dispersoids, which depends critically on the homogenisation, hot rolling and solution treatment characteristics

(iii) the change in strength and strain hardening rate induced by the quench related microstructural changes are small and do not appear to a have a direct influence on the notch resistance of the alloy.

Conclusion

The compositional change from alloy 7040 to alloy 7050 improves the yield stress – notch resistance combination by reducing both the strength loss and the loss in notch resistance associated with a decrease in quench rate. This improvement is largely related to a reduction in the alloy sensitivity to heterogeneous precipitation on dispersoids. When present, these precipitates deplete the solid solution (and therefore decrease the attainable yield strength) and decrease the intrinsic toughness of the grain interiors by favouring early ductile fracture. However, alloy 7040 still shows a strong decrease in notch resistance after a slow quench, mainly because of quench-induced grain boundary precipitates. Further optimisation of this property compromise needs a better understanding of the effect of alloy composition and quench path on the kinetics of grain boundary precipitation.

Acknowledgements

Dr F. Livet and Dr F. Bley are gratefully acknowledged for their valuable help with the Ultra-Small Angle X-ray Scattering experiments. Dr A. Bigot and V. Chastagnier are warmly thanked for their help with the FEG-SEM analysis. ANRT is acknowledged for providing part of the funding for the PhD grant of one of the authors (DD).

References

1. J. FIELDING: 'Introduction to aircraft design'; 1999, Cambridge, Cambridge University Press.
2. I. POLMEAR: 'Light alloys'; 1995, London, Edward Arnold
3. N. U. DESHPANDE, A. M. GOKHALE, D. K. DENZER and J. LIU: *Metall. Mater. Trans.*, 1998, **29A**, 1191.
4. B. MORERE, J. C. EHRSTRÖM and P. J. GREGSON: *Metall. Mater. Trans.*, 2000, **31A**, 2503.
5. N. KAMP, I. SINCLAIR and M. J. STARINK: *Metall. Mater. Trans.*, 2002, **33A**, 1125.
6. P. GUYOT and L. COTTIGNIES: *Acta Mater.*, 1996, **44**, 4161.
7. A. DESCHAMPS, S. ESMAEILI, W. J. POOLE and M. MILITZER: *J. Phys. IV*, 2000, **10**, PR6, 151 (Proc. 6th Japan – France Materials Science Seminar, 1999, Poitiers, France). 4 5
8. G. G. GARRET and J. F. KNOTT: *Metall. Trans.*, 1978, **9A**, 1187.
9. C. Q. CHEN and J. F. KNOTT: *Metall. Sci.*, 1981, **15**, 357.
10. A. T. ZEHNDER and C. Y. HUI: *Scripta Mater.*, 2000, **42**, 1001.
11. T. PARDOEN and J. W. HUTCHINSON: *J. Mech. Phys. Solids*, 2000, **48**, 2467.
12. J. D. EMBURY and E. NES: *Z. Metallk.*, 1974, **65**, 45.
13. E. HORNBOGEN and M. GRÄF: *Acta Metall.*, 1977, **25**, 877.
14. T. KAWABATA and O. IZUMI: *Acta Metall.*, 1976, **24**, 817.
15. A. K. VASUDÉVAN and R. D. DOHERTY: *Acta Metall.*, 1987, **35**, 1193.
16. B. Q. LI and A. P. REYNOLDS: *J. Mater. Sci.*, 1998, **33**, 5849.
17. A. DESCHAMPS and Y. BRÉCHET: *Mater. Sci. Eng.*, 1998, **A251**, 200.
18. J. T STALEY, R. D. DOHERTY and A. P. JAWORSKI: *Metall. Trans.*, 1993, **24A**, 2417.
19. R. C. DORWARD and C. BOUVIER: *Mater. Sci. Eng.*, 1998, **A254**, 33.
20. G. M. RAYNAUD, P. LASSINCE and R. MACE: *Aluminium World*, 2001, **2**, 97 – 99.
21. R. SHAHANI, T. WARNER, C. SIGLI, P. LASSINCE and P. LEQUEU: Proc. 6th Int. Conf on 'Aluminium alloys', Toyohashi, Japan, 1105; 1998, Tokyo, Japan Institute of Light Metals.
22. P. SAINFORT, C. SIGLI, G. M. RAYNAUD and P. GOMIERO: Proc. 5th Int. Conf on 'Aluminium alloys', Grenoble, France, 1996, *Mater. Sci. Forum*, 1997, **242**, 25.
23. F. HEYMES, B. COMMET, B. DUBOST, P. LASSINCE, P. LEQUEU and G. M. RAYNAUD: Proc. 1st Int. Conf. on 'Non-ferrous processing and technology', St Louis, USA, 249; 1997, Materials Park, OH, ASM International.
24. A. DESCHAMPS, Y. BRECHET and F. LIVET: *Mater. Sci. Technol.*, 1999, **15**, 993.
25. G. G. GARRET and J. F. KNOTT: *Metall. Trans.*, 1978, **9A**, 1187.
26. J. G. KAUFMAN and A. F. KNOLL: *Mater. Res. Std.*, 1964, **4**, 151.
27. H. D. DUDGEON, N. C. PARSON, S. A.COURT and R. A. RICKS: Proc. 4th Int. Conf. on 'Aluminum alloys', Atlanta, GA, USA, Vol. 1, 443; 1994, Georgia Institute of Technology.
28. D. DUMONT, A. DESCHAMPS and Y. BRÉCHET: *Mater. Sci. Eng.*, 2003, **A356**, 326.
29. G. T. HAHN and A. R. ROSENFIELD: *Metall. Trans. A*, 1975, **6A**, 653.
30. P. ACHON, J. C. EHSTROM and A. PINEAU: *J. Phys. IV*, 1996, **6**, C6 – 3.
31. A. DESCHAMPS and Y. BRÉCHET: *Scripta Mater.*, 1998, **39**, 1517.
32. H. LÖFFLER, I. KOVÁCS and J. LENDVAI: *J. Mater. Sci.*, 1983, **18**, 2215.

33. A. DESCHAMPS, Y. BRÉCHET and F. LIVET: *Acta Mater.*, 1999, **47**, 281.
34. U. F. KOCKS: *J. Eng. Mater. Technol.*, 1976, **98**, 76.
35. H. MECKING, B. NICKLAS, N. ZARUBOVA and U. F. KOCKS: *Acta Metall.*, 1986, **29**, 1865.
36. A. DESCHAMPS, M. NIEWCZAS, F. BLEY, Y. BRECHET, D. EMBURY, L. LESINQ and F. LIVET: *Phil. Mag.*, 1999, **A79**, 2485.
37. I. KIRMAN: *Metall. Trans.*, 1971, **2**, 1761.
38. C. Q. CHEN and J. F. KNOTT: *Metall. Sci.*, 1981, **15**, 357.
39. M. LI and J. F. BUTLER: Proc. Conf. on 'Integration of material, process and product design', Seven Springs, PA, USA, 47; 1998, Rotterdam, Balkema.
40. D. H. BRATLAND, ¿. GRONG, H. R. SHERCLIFF, O. R. MYHR and S. TKOTTA: *Acta Metall.*, 1997, **45**, 1.
41. J. T. STALEY: *Mater. Sci. Technol.*, 1987, **3**, 923.

MST *(gamma)* MST38227.3d 9/3/04 18:11:17 Rev 7.51n/W (Jan 20 2003)